Available online at www.sciencedirect.com
SCIENCE DIRECT®

Nuclear Science and Techniques, Vol.17, No.6 (2006) 389–395

NUCLEAR SCIENCE AND TECHNIQUES

2D and 3D refraction-based visualization of breast cancer for early clinical check

Masami ANDO[1,2,3*] Anton MAKSIMENKO[2] Tetsuya YUASA[4] Eiko HASHIMOTO[2] Katsuhito YAMASAKI[5] Shu IHIHARA[6] Hiroshi SUGIYAMA[2,3] Tokiko ENDO[7] LI Gang[8] CHEN Zhihua[9], Kazuyuki HYODO[2], Ei UENO[10]

([1]DDS Center, RIST, Tokyo University of Science, Chiba 278-8510, Japan;

[2]Photon Factory, IMSS, KEK, Oho 1-1, Tsukuba, Ibaraki 305-0801, Japan;

[3]Department of Photo-Science, GUAS, Oho 1-1, Tsukuba, Ibaraki 305-0801, Japan;

[4]Faculty of Engineering, Yamagata University, Yonezawa, Yamagata 992-8510, Japan;

[5]Clinical Genome Informatics Center, School of Genome Science, Kobe University, Hyogo 650-0017, Japan;

[6]Department of Pathology, Nagoya Medical Center, Nagoya 460-0001, Japan;

[7]Department of Radiology, Nagoya Medical Center, Nagoya 460-0001, Japan;

[8]BSRF, IHEP, CAS, Yuquanlu, Beijing 100049, China;

[9]China-Japan Friendship Hospital, Yinhua Donglu, Beijing 100029, China;

[10]Department of Breast-Thyroid-Endocrine Surgery, University of Tsukuba, Ibaraki 305-8573, Japan)

Abstract Ductal carcinoma in-situ (DCIS) has been visualized by 2D XDFI (X-ray dark-field imaging) and further by a 3D X-ray CT, and the data was acquired by the X-ray optics DEI (diffraction-enhanced imaging). A newly made algorithm was used for CT. Data of 900 projections with interval of 0.2 degrees were used. Ductus lactiferi, microcalcification in a 3D form have been clearly visible. The spatial resolution available was approximately 30 μm.

Key words X-ray dark-field imaging (XDFI), Ductal carcinoma in-situ (DCIS), Diffraction-enhanced imaging (DEI), Microcalcification, 3D CT, Synchrotron radiation, Vertical wiggler, X-ray refraction, Monochrocollimator

CLC numbers R814.42, R737.9, R730.44

1 Introduction

Breast cancer is a leading cause of cancer death worldwide. In Japan, almost 4% of the females are at a risk of suffering from breast cancer. Using epidemiological analysis on the correlation between mammography and mammotome biopsy H. Hashimoto [1] at Chiba Foundation for Health Promotion and Disease Prevention classified breast cancer with calcification into five groups: In group # 5, cancer has been detected with a probability of 18 out of 19 patients, corresponding to 94.7% ratio, with highly suggestive malignancy. In group # 4, cancer has been detected with a probability of 53 out of 89 patients, corresponding to 59.6% ratio, with suspicious malignancy cancer. In group # 3, cancer has been detected with a probability of 40 out of 366 patients, corresponding to 10.9% ratio, with benign cancer, but with malignancy that cannot be ruled out. Among the breast cancer confirmed by biopsy, 18 patients come from group # 5 corresponding to 15.7% of all the patients, 53 from group # 4, corresponding to 46.1% of all the patients, and 40 from # 3, corresponding to 38.2% of all the patients, respectively.

*E-mail: masami.ando@kek.jp

Summarizing this data one can say that only 15.7% of the patients with breast cancer, having calcification, can be clearly diagnosed as having breast cancer, by detection of fine linear calcification or pleomorphic calcification in the linear and/or segmental area. Breast cancer death comprises approximately 15% - 20% of all cancer deaths. As early detection of breast cancer usually gives a good prognostic outcome, it is a key to prevent death on account of breast cancer. Mammography together with ultrasonography, as an early check, is one of the powerful screening modalities. Since the discovery of X-ray by Roentgen in 1895, all X-ray medical imaging, including mammography, in hospitals around the world, have been purely based on absorption contrast. Nevertheless, limitation in their spatial and contrast resolutions exists in early detection. As breast cancer is not necessarily visible with absorption contrast, one needs alternative methodology for visualizing breast cancer, with higher contrast and higher spatial resolution.

Following a pioneering study on imaging of breast cancer by Burattini's group [2] a trial to visualize breast cancer tissue has been performed by PCI, [3, 4] DEI, [5 - 7] PIC (phase-interference contrast), [8] the super magnification imaging (SMI), [9, 10] DFI, [11, 12] and XRF (X-ray fluorescence) [13].

2 Observation by X-ray dark field imaging (XDFI)

Here a 2D projected XDFI [11, 12] is proposed that will be used for clinical diagnosis. The X-ray optics XDFI [11, 12] is characterized as shown in Fig.1. This is a double crystal arrangement with a Laue type angular analyzer with a specified thickness, to allow only refracted components to pass through to an imaging detector. In this article, XDFI [11, 12] has been used for an overall survey of a DCIS specimen.

A specimen of a breast DCIS has been chosen from 'c' as shown in Fig.2. This indicates a variety of tissues such as distorted linear structure, healthy, and malignant tissue. Object **s(w)** has been angularly analyzed by **k(w),** which has a specified thickness of 2.124 mm for 35 keV, hence only ***r(w)*** will be able to pass through **k(w)** in the forward direction. This picture clearly delineates distorted linear structure and ductus lactiferi. A specimen with the diameter of 3.5 mm and depth of 4.7 mm was punched out at the place shown with the label 'c' in Fig. 2. This has been used to show 3D CT.

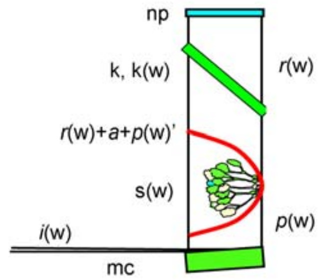

Fig.1 X-ray optics of DFI. A specimen **s(*w*)** DCIS was illuminated by plane wave ***p(w)*** that was made by the mono-chro-collimator **mc**. **k** is a Laue case analyzer with special thickness of 2.124 mm for 35 keV. The diffracting planes of mc and **k** are 220 in a parallel arrangement. The beam carrying both information ***r*(*w*)** because of refraction, and ***a*** because of absorption of the sample, and the partial illuminating light ***p(w),*** has been analyzed by **k** with a function of **k(w)**. Only the refracted component ***r(w)*** can pass through **k(w)** as the DF image that is stored in **np** nuclear plate.

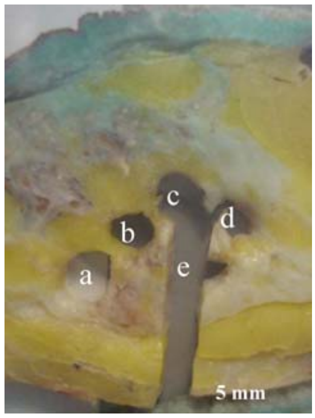

Fig.2 A DCIS (ductus carcinoma in situ) specimen with thickness of 4.7 mm. The field has a dimension of 24.5 mm x 31 mm showing skin tissue in blue-green color, fatty tissue in yellow color, normal mammary tissue in white color and cancer in gray color. The gray area is hard to touch. A rod shaped specimen with size of 3.5 mm in diameter and 4.7 mm in length was punched out from the mark 'c'. 'a', 'b', 'd' and 'e' are other marks from where other specimens were taken out. The whole area shown in this figure corresponds to DCIS.

In Fig. 3 an XDF image is shown, where a – d shows holes corresponding to those in Fig. 2. A lineage image and holes a-e corresponding to those in Fig. 2 are shown. A lineage structure probably ductus lactiferi marked with 'dl' is also seen. The XDF image should involve a great deal of information on the internal structure of the DCIS, whereas the photo in Fig. 2 only shows the surface.

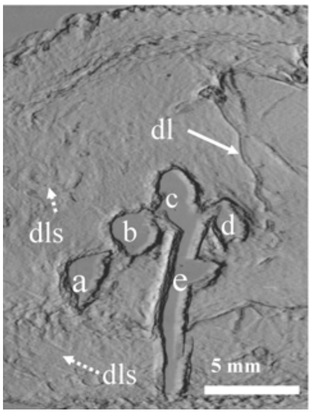

Fig.3 DF image of the specimen shown in Fig. 1 taken with the X-ray optics shown in Fig.2. Labeled marks ‘a’, ‘b’, ‘c’. ‘d’ and ‘e’ are the positions where the specimens have been taken out by punching. Their edges are enhanced by refraction. The X-ray energy used was 35 keV. ‘dls’ corresponds to distorted linear structure characterized as malignancy and ‘dl’ shows a linear structure of ductus lactiferi that was not visualized in Fig. 1 presumably because it locates underneath the surface.

3 Mathematical algorithm for 3-D reconstruction

The algorithm for 3D CT that has been developed here is characterized by a complex expression of a refraction angle. It is well known that conventional absorption based X-ray imaging, delineates an object because of a difference of X-ray absorption cross section that has relation to an imaginary part of the complex refractive index $n = 1 - \tilde{n} + \mathrm{i}\kappa$. However, κ of low atomic-number elements in soft tissue of biomedicine comprising hydrogen, carbon, nitrogen, and oxygen, cannot produce sufficient contrast because $\kappa \approx 0$. In case of visualizing such objects with hard X-rays, for instance in clinical application, it is much more advantageous to detect variations of the propagation direction of the incident X-rays using an analyzer with high angular sensitivity over conventional absorption contrast.

So far a variety of imaging schemes for a phase object have been proposed [14 - 25]. Maksimenko *et al.*, have recently proposed a novel tomographic imaging protocol based on a physico-mathematically defined reconstruction algorithm [22 - 25], with a paraxial-ray approximation in the domain of geometrical optics. This has experimentally obtained a satisfactory result. The principle is outlined with the ray equation as follows:

$$\frac{\mathrm{d}}{\mathrm{d}s}\, n(\boldsymbol{r})t(\boldsymbol{r}) = \nabla \mathrm{n}(\boldsymbol{r}) \tag{1}$$

where $\boldsymbol{r}$ is a spatial coordinate, $n(\boldsymbol{r})$ is a refractive index distribution, $t(\boldsymbol{r})$ is a unit tangential vector of ray propagation, and s is an arc length parameter. Executing the differentiation of LHS (light hand side),

$$n\frac{\mathrm{d}\alpha}{\mathrm{d}s}\boldsymbol{v} + \frac{\mathrm{d}n}{\mathrm{d}s}\boldsymbol{t} = \nabla n \tag{2}$$

where $\boldsymbol{v}$ is a unit normal vector, and α is an angular deflection from the propagation direction, satisfying the following relationship from differential geometry: $\mathrm{d}\boldsymbol{t}/\mathrm{d}s = (\mathrm{d}\alpha/\mathrm{d}s)\ \boldsymbol{v}$. Therefore, two independent equations have been derived:

$$\begin{aligned} \frac{\mathrm{d}\tilde{n}}{\mathrm{d}s} &= \nabla\tilde{n}\cdot\boldsymbol{t} \\ \frac{\mathrm{d}\alpha}{\mathrm{d}s} &= \nabla\tilde{n}\cdot\boldsymbol{v} \end{aligned} \tag{3}$$

where the approximation of $\tilde{n} << 1$ is used.

Next, the so-called classical CT measurement configuration was considered. The xy-coordinate system is fixed to an object and is rotated by θ around the origin to obtain the pq-coordinate system. Under the paraxial-ray approximation because $n \approx 1$, line integral was executed on line l of Eq. (3) to obtain

$$\nabla\tilde{n}\,(r)\boldsymbol{t}\mathrm{d}s = \sum_{-\infty}^{\infty} |\nabla\tilde{n}\,(r_i)|\cos\varphi\,(r_i)\text{-}\theta\mathrm{d}q \approx 0 \tag{4}$$

$$\nabla\tilde{n}\,(r)\,\boldsymbol{v}\mathrm{d}s = \sum_{-\infty}^{\infty} |\nabla\tilde{n}\,(r_i)|\sin\varphi\,(r_i)\ \text{-}\theta\mathrm{d}q \approx \alpha(p,\theta) \tag{5}$$

where $r_i = p\cos\theta - q\sin\theta,\ p\sin\theta + q\cos\theta$, and $\varphi(r_i)$ is an angle between $\nabla\tilde{n}$ and the x-axis. From Eqs. (4) and (5), the following equation is obtained:

$$\mathrm{i}\alpha(p,\theta)\exp(\mathrm{i}\theta) = \sum_{-\infty}^{\infty} |\nabla\tilde{n}\,(r_i)|\exp(\mathrm{i}\varphi\,(r_i))\mathrm{d}q \tag{6}$$

that is a complex-valued version of the Radon transform [26]. Maksimenko *et al.*, devised a complex-valued algorithm of filtered back projection to solve the inverse problem, that is, image reconstruction from complex-valued projections that has led to the vector field $\nabla\tilde{n}$ and finally the refractive index distribution. In addition, they first succeeded in the experimental implementation of the algorithm to reconstruct a simple structure [22] that happened to involve a small crack [23], which was otherwise not visible.

4 Observation by 3-D reconstruction

A technique of CT reconstruction because of X-ray refraction needs angularly well resolvable X-ray optics that can detect an extremely small deflection angle at the order of a few times of $10^{-6} \sim 10^{-7}$. Furthermore, one needs an algorithm for CT reconstruction. In Fig. 4 an X-ray optics is shown which is used to obtain appropriate data for 3D reconstruction. That comprises a monochromator- collimator **MC(w)** and an angular analyzer **K(w)**. A specimen on a rotating axis for data acquisition locates in between **MC(w)** and **K(w)**. The incident beam ***i*(*w*)** is mono-chro-collimated by **mc** to produce plane wave ***p*(*w*)**. Angular information of **s(w)** of objects will produce ***r*(*w*) + a**. This will be angularly analyzed by **k** that has an angular analytical power **K(w)**. Chapman *et al*'s DEI (diffraction enhanced imaging) [17] has been adopted to deduce a pure refraction component so that each data set for a fixed angle θ was taken at both wings of the rocking curve at w = - 0.5 left and at w = + 0.5 where w means the angular parameter and w = 1 covers the full angular range. A sample was remotely rotated every $\Delta\theta$, which was 0.2°. **mc** was asymmetrically cut [27] Si (220) with α = 9.5° where α was the angle between the surface and the diffracting planes. **K(w)** was a symmetric Si (220) one. The energy used in the experiment was 11.7 keV. A specimen used in this experiment was a rod shaped invasive DCIS. Data was acquired on either flank of the rocking curve with a smooth slope [17].

The number of sample rotations for data acquisition in the experiment was 900. It took 200 ms ~ 1 s for data acquisition of each frame, 2 - 5 seconds for data transfer to the pc and 1 s for sample rotation and additional 1 s for stabilizing the system free from vibration, because of the motor. Every ten data acquisitions the X-ray intensity by CCD was measured, without specimen, for background subtraction. A CCD Camera X-FDI 1.00:1, the type with air cooling, which has a view size of 8.7 mm (h)×6.9 mm (v), was supplied by Photonic Science which is compatible with 16-bit and 1392×1040 pixels with pixel size of 6.3 μm×6.6 μm. Data transfer was done by FireWire (IEEE 1394). After this series of measurement was done the angular position of the analyzer crystal was changed from either angle to continue the other series of measurement. In total the data acquisition time was approximately three hours.

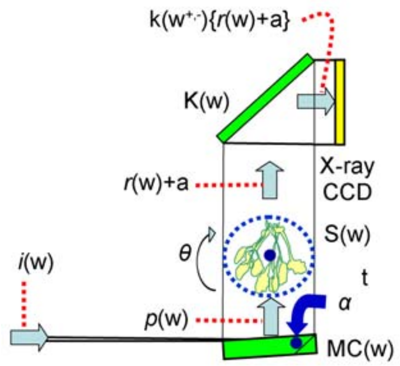

Fig.4 Schematic of the DEI optics to acquire data for 3D reconstruction. A specimen **s(w)** DCIS was rotated every $\Delta\theta$ = 0.2° around the axis from 0° to 180°. **mc** means a monochro-collimator that converts the incident beam ***i*(*w*)** into almost plane wave ***p*(*w*)**. **K(w)** is a Bragg case analyzer. The diffracting planes of **MC(w)** and **K(w)** are (220) in a parallel arrangement. The beam carrying both information ***r*(*w*)** because of refraction and ***a*** because of absorption of the sample has been analyzed by **K(w)**. Two images both sides (+,-) of the flank of the rocking curve for each θ in Eq. (6) are stored in a CCD camera.

According to Maksimenko *et al*'s algorithm [22 - 25], sinogram is used as the input function for the CT reconstruction algorithm. To evaluate the spatial resolution of the system one has to consider four factors: the source size, the ratio of the distance between the source and the object to that between the object and the CCD detector, how much refraction takes place, and the pixel size of the CCD detector. In the current experiment, as the order of refraction ranges around $10^{-6} \sim 10^{-7}$, the beam deflection may take place after reaching the CCD camera at the order of 5 μm if the distance between the object and the CCD detector is 25 cm so that one does not have to worry about cross talk at CCD. A series of 900 projected images for reconstructing a 3D image were acquired.

This modality has been applied to soft tissue. [28 - 31] In Fig. 5, reconstructed CT images are shown. The right bottom figure shows the outer surface, whereas three others show each cross-sectioned one as shown in the right bottom figure. High contrast is seen in the center of the milk duct. These areas are considered as calcifications. Low contrast areas are seen adjacent to the calcification area. These are considered as the necrotic ones. Higher contrast areas are seen surrounding the outside of the low contrast necrotic areas. These are considered as cancer cell layers spreading inside milk ducts. High contrast linear areas or net-like areas are seen outside the milk duct. These structures are considered as invasive cancer cell areas in the interstitial tissue. Especially the # 3 milk duct seen in the blue image is almost closed. Further one can easily recognize that most of the milk ducts hold fringes surrounding the ducts. These white structures mean more electron density. Even as their extension invasive carcinoma with irregular shape is clearly shown.

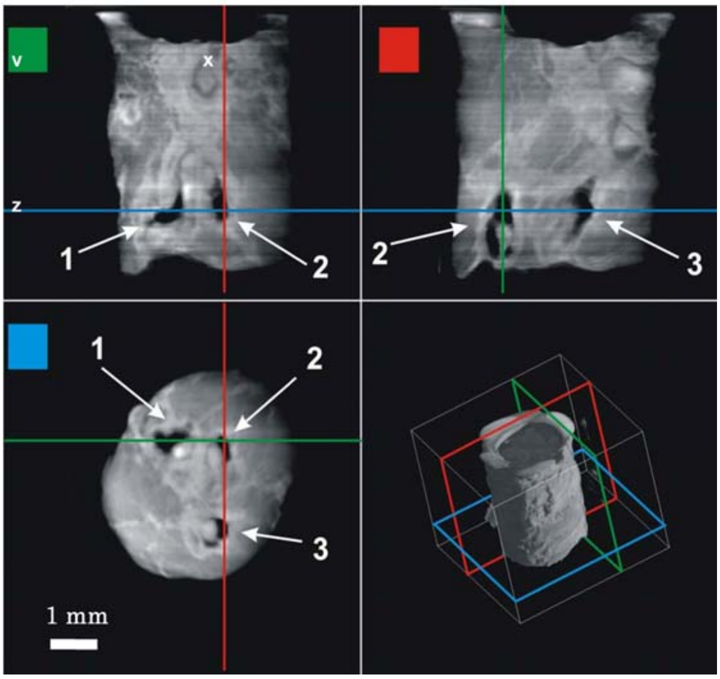

Fig.5 Reconstructed 3D image of a DCIS is shown in the bottom right together with three color frames, red (x-plane), green (y-plane) and blue (z-plane). The picture at the left bottom shows cross sections of three milk ducts with the number 1, 2 and 3. In almost all of them are seen microcalcifications and higher contrasts at each fringe and finally extension of invasive carcinoma.

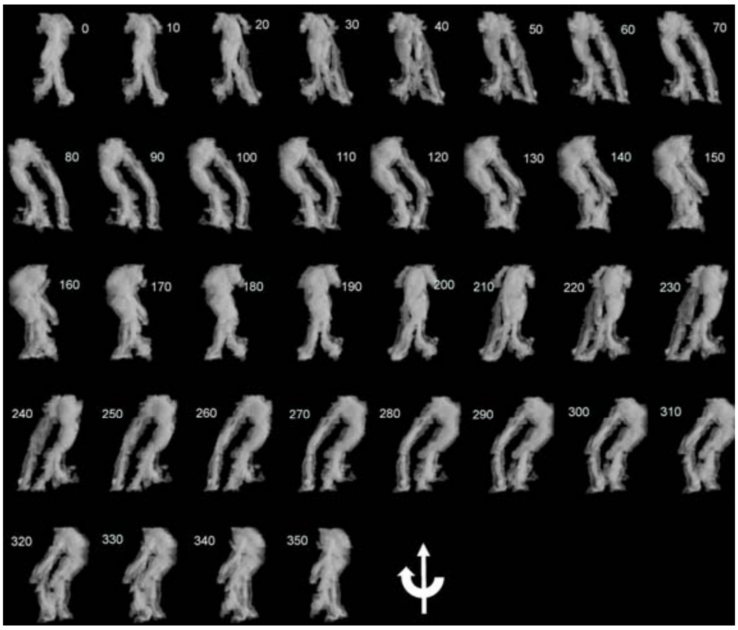

Fig. 6 36 pictures of reconstructed DCIS. This shows rotation of the DCIS seen in Fig. 5. Each view is arranged with every 10 degrees of rotation. The pictures shown here are milk ducts that contain calcification inside. Tissues around the milk ducts have been removed for better view. Walls of the milk ducts are soft tissue that have not been visible by absorption contrast.

In Fig. 6 is shown a movie [31] that means a series of rotating images of milk ducts containing calcification of the reconstructed DCIS. Each shows a milk duct wall and calcification inside the milk duct. The number either on the right hand side or on the left hand side indicates the rotation angle with interval of 10 degrees so that 36 pictures mean a full 360 degrees rotation around the axis shown at the bottom. This shows that calcification continues from the bottom up to the top corresponding to the direction of the nipple.

5 Result and discussion

Mammography is quite significant to discover breast cancer at its early stage; and the size of the cancer that is able to be discovered by the current technique is around 1 cm. By further development of the technique described in this note the size of the cancer that is able to be found could be much smaller ~ say around 250 m or even smaller. The current mammography has an important role as an indicator of adequacy of breast cancer treatment. [32, 33]. Also magnified mammography seems far more useful in recognizing the tumor extent than conventional mammography [34] because of its much higher spatial resolution, around 5-10 m, whereas, the conventional absorption one provides something worse than 50 m. Also refraction based mammography has a higher grade potential of diagnosis compared to the conventional mammography. The 2-D XDFI would be suitable for a novel type of mammography and 3-D CT for overall precision diagnosis in case of solving a skin radiation dose.

Acknowledgements

The synchrotron experiment was performed at the Photon Factory with the approval from KEK (Proposal Numbers were #2002G045 and #2005G085). The research was conducted by the financial support from the MEXT (Grant-in-Aid for Exploratory Research #15654042, Grant-in-Aid for JSPS Fellows #1705335 and Grant-in-Aid for Scientific Research (A) #18206011) and also from the 2004 Suzuken Research Fund and the 2006 Horiba Special Award. The necessary process of acquiring consent from the patient has been obtained.

References

1 Hashimoto H, Clinical Imagiology, 2002, **9**:937.

2 Burattini E, Cossu E, Di Maggio C, *et al*. Radiology, 1995, **195**:239.

3 Johnston R E, Washburn D, Pisano E, *et al*. Radiology. 1996, **200**:659.

4 Chapman D, Pisano E, Thomlinson W, *et al*. Breast Disease. 1998, **10**:197.

5 Di Michiel M *et al*. in: Medical Applications of Synchrotron Radiation, Ando M and Uyama C (eds.), Tokyo: Springer-Verlag, 1998:78.

6 Arfelli F *et al*. Radiology. 2000, **215**:286.

7 Hasnah M O, Zhong Z, Oltulu O, *et al*. Med. Phys. 2002, **29**:2216.

8 Takeda T, Wu J, Tsuchiya Y, *et al*. J. J. Appl. Phys. 2004, **43**:5652.

9 Toyofuku F, Higashida Y, Tokumori K, *et al*. J. J. Med. Phys. 2003, **23(Supp.3)**: 127.

10 Toyofuku F, Higashida Y, Tokumori K, *et al*. J. J. Med. Phys. 2004, **24(Supp.3)**: 378.

11 Ando M, Sugiyama H, Maksimenko A, *et al*. Jpn. J. Appl. Phys. 2002, **41**:L1016.

12 Ando M, Yamasaki K, Toyofuku F, *et al*. Jpn. J. Appl. Phys. 2005, **44**:L528.

13 Ando M, Yamasaki K, Ohbayashi C, *et al*. Jpn. J. Appl. Phys. 2005, **44**:L998.

14 Podurets K M, Somenkov V A, Shil'shtein S Sh, Physica. 1989, **B156-157**:691.

15 Ingal V N, Beliaevskaya E A, J. Phys. D: Appl. Phys. 1995, **28**:2314.

16 Davis T J, Gao D, Gureyev T E, *et al*. Nature. 1995, **373**:595.

17 Chapman D, Thomlinson W, Johnston R E, *et al*. Phys. Med. Biol. 1997, **42**:2015.

18 Yagi N, Suzuki Y, Umetani K, *et al*. Med. Phys. 1999, **26**:2190.

19 Momose A, Takeda T, Itai Y, *et al*. Nature Medicine. 1996, **2**:1434.

20 Hirano K, Maksimenko A, Sugiyama H, *et al*. Jpn. J. Appl. Phys. 2002, **41**:L595.

21 Maksimenko A, Sugiyama H, Hirano K, *et al*. Measurement Science and Technology. 2004, **15**:1251.

22 Maksimenko A, Ando M, Sugiyama H, *et al*. Appl. Phys. Lett. 2005, **86**:124105-1.

23 Maksimenko A, Ando M, Sugiyama H, *et al*. Jpn. J. Appl. Phys. 2005, **44**:L633.

24 Yuasa T, Maksimenko A, Hashimoto E, *et al*. Optics Letters. 2006, **31**:1818.

25 Yuasa T, Sugiyama H, Zhong Z, *et al*. JOSA. 2005, **22**:2622.

26 Kaka A C, Slaney M, Principles of computerized tomographic imaging, New York: IEEE Press, 1988.

27 Kohra K, J. Phys. Soc. Jpn. 1962, **17**:589.

28 Ando M, Maksimenko A, Yuasa T, *et al*. Bioimages. 2006, **13** :1.

29 Hashimoto E, Maksimenko A, Sugiyama H, *et al*. Zoological Society. 2006, **23 :**in press.

30 Yuasa T, Hashimoto E, Maksimenko A, *et al*. submitted.

31 Ando M, Maksimenko A, Hashimoto E, *et al.* submitted.

32 Sadowsky N L, Semine A, Harris J R, Cancer. 1990, **65** :2113.

33 Gluck B S, Dershaw D D, Liberman L, *et al*. Radiology 1993, **188**:469.

34 Marrow M, Schmidt R, Hassett C, Surgery. 1995, **118**:621.